Nanomagnetic Sensing of Blood Plasma Protein Interactions with Iron Oxide Nanoparticles: Impact on Macrophage Uptake

Lénaic Lartigue,[†] Claire Wilhelm,[†] Jacques Servais,[†] Cécile Factor,[‡] Anne Dencausse,[‡] Jean-Claude Bacri,[†] Nathalie Luciani,[†] and Florence Gazeau[†,*]

[†]Laboratoire Matière et Systèmes Complexes (MSC), UMR 7057 CNRS/Université Paris—Diderot, PRES Sorbonne Paris Cité, 75205 Paris cedex 13, France and [‡]GUERBET, BP57400, 95943 Roissy CdG Cedex, France

ABSTRACT One of the first biointeractions of magnetic nanoparticles with living systems is characterized by nanoparticle—protein complex formation. The proteins dynamically encompass the particles in the protein corona. Here we propose a method based on nanomagnetism that allows a specific *in situ* monitoring of interactions between iron oxide nanoparticles and blood plasma. Tracking the nanoparticle orientation through their optical birefringence signal induced by an external magnetic field provides a quantitative real-time detection of protein corona at the surface of nanoparticles and assesses eventual onset of particle aggregation. Since some of the plasma proteins may cause particle aggregation, we use magnetic fractionation to separate the nanoparticle clusters (induced by "destabilizing proteins") from well-dispersed nanoparticles, which remain isolated due to a stabilizing corona involving other different types of proteins. Our study shows that the "biological identity" (obtained after the particles have interacted with proteins) and aggregation state (clustered *versus* isolated) of nanoparticles depend not only on their initial surface coating, but also on the concentration of plasma in the suspension. Low plasma concentrations (which are generally used *in vitro*) lead to different protein/nanoparticle complexes than pure plasma, which reflects the *in vivo* conditions. As a consequence, by mimicking *in vivo* conditions, we show that macrophages can perceive several different populations of nanoparticle/protein complexes (differing in physical state and in nature of associated proteins) and uptake them to a different extent. When extrapolated to what would happen *in vivo*, our results suggest a range of cell responses to a variety of nanoparticle/protein complexes which circulate in the body, thereby impacting their tissue distribution and their efficiency and safety for diagnostic and therapeutic use.

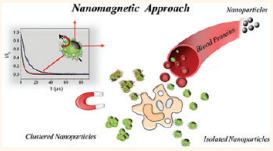

KEYWORDS: bionanointeractions · nanomagnetism · nanomedicine · superparamagnetic iron oxide nanoparticles · blood plasma · mononuclear phagocyte system

Understanding the interactions of nanomaterials with the biological environment has crucial implications for both the efficacy of nanomedicines and safety issues in nanotechnology. After entering into the bloodstream, nanoparticles interact with biomolecules forming a "bionano interface". At this interface a protein corona results from a dynamic exchange with biomolecules, influencing both the surface state and the local organization of nanoparticles.[1−4] Therefore what the cells "see and process" are no longer the initially engineered nanoparticles, but the dynamic biomolecule—nanoparticle complexes which are formed *in vivo*.[5] The biodistribution and fate of nanoparticles in the organism will significantly depend on their early interactions with plasma proteins.[6]

Among the variety of nanoparticle functionalities, magnetic properties paved the way for various diagnostic and therapeutic applications such as magnetic resonance imaging (MRI), magnetic targeting, magnetically induced hyperthermia, triggered drug release or magnetic control of cell migration and signaling.[7] Remarkably, all these applications rely on the on-command actuation of nanoparticles by different magnetic stimuli applied at a distance and can be combined together to design theranostic nanoplatforms.[8,9] However, for most of the magnetic nanoparticles, the relatively poor control of their interactions with blood constituents remains a challenging obstacle toward their efficient targeting to specific organs or cells. The primary target of such nanoparticles are macrophages, which can be detected and tracked by MRI, allowing the monitoring of their recruitment into inflamed tissues such as atherosclerotic plaques, adipose tissue, brain ischemia, or tumors.[10−13] Macrophage imaging in various diseases like, for example, the metabolic syndrome, atherosclerosis, stroke, multiple sclerosis, Alzheimer disease, or cancer is one of the most promising goals sought by nanomedicine, using superparamagnetic iron oxide nanoparticles as *in vivo* MRI markers.[14]

* Address correspondence to florence.gazeau@univ-paris-diderot.fr.

Received for review January 5, 2012 and accepted February 10, 2012.

Published online February 10, 2012
10.1021/nn300060u

However while some types of nanoparticles will mainly accumulate in resident macrophages of liver and spleen, others may preferentially target circulating monocytes and recruited macrophages involved in inflammation processes.[12,15−17] Moreover, macrophages are proposed as potent cellular vectors for delivery of therapeutics, including nanoparticle-based ones, into their homing sites.[18−20] Surface state and protein corona of nanoparticles are suggested to play a key role in determining their circulation time, notably by governing the processes of phagocytosis (i.e., determining which type of mononuclear phagocytes will uptake the particles and at which rate). Nevertheless the precise underlying mechanisms of the nanoparticle fate are not fully clarified. A better understanding of nanoparticle interactions with plasma proteins and their effect on cell capture should help to improve the control of their biodistribution and optimize nanoparticles for a desired application.

Besides, among other impacts the protein corona might have, recent studies reported that the way nanoparticles interact with biological matter affects their magnetic properties *via* surface modifications, aggregation, or cell confinement. In turn, the biological environment deeply modifies particle efficiency as MRI contrast agents or therapeutic nanomediators.[21,22] Therefore the formation of nanoparticle−protein complexes must be taken into account when tailoring efficient as well as safe magnetic nanoparticles.[23]

While adsorption of proteins on magnetic nanoparticles has been reported in several studies,[24−28] quantitative investigations of their dynamic interactions with plasma constituents and its consequence on macrophage uptake are still scarce. Therefore we here report a method based on nanomagnetism to specifically quantify, *in situ* and in real time, the coupling of macromolecules to magnetic nanoparticles in blood plasma. Furthermore, this method allows the detection of the onset of nanoparticle aggregation. Beyond currently used analytical techniques, which are not specific to nanoparticles, the nanomagnetic technique that we propose in this work directly relies on magneto-optic properties of the investigated nano-objects and thus demonstrates an enhanced sensitivity and specificity to conformational or organizational changes occurring at the nanoscale. Moreover, to identify the proteins at the nanoparticle surface, we used their magnetic properties to separate nanoparticles from the protein dispersion without centrifugation, thus avoiding the loss of weakly bound proteins. Finally, we quantified the interactions of the identified nanoparticle−protein complexes with monocyte-derived macrophages by means of single cell magnetophoresis. The combination of these magnetically based methods allows an in-depth investigation of the plural biological identities and physical states of magnetic nanoparticles as a function of their initial surface coating and their biological environment, as well as the relationship between the displayed identity and macrophage uptake.

TABLE 1. Physicochemical Characterization of Bare Studied Nanoparticles

			magnetization[a]		DLS[b]		Birefringence	
sample	d_{TEM} (nm)	ξ (mV)	d_{magn} (nm)	σ	d_H (nm)	PDI	d_H (nm)	α
citrate-coated	7.0 ± 2.0	−31.6	6.5	0.33	20.4	0.166	21.1	0.70
Pi903	6.9 ± 1.8	−52.2	7.2	0.24	19.7	0.361	20.7	0.69
P904	6.7 ± 1.6	−37.4	7.2	0.24	25.6	0.274	20.9	0.70

[a] The magnetic size distribution (log-normal distribution with characteristic diameter d_{magn} and polydispersity index σ) is deduced from the magnetization curve at room temperature. [b] PDI= polydispersity index determined by DLS.

RESULTS AND DISCUSSION

Characterization of Iron Oxide Nanoparticles with Different Surface Coatings. To investigate plasma interactions with well-defined magnetic nanoparticles of biomedical interest (currently evaluated in preclinical trials), we chose iron oxide nanoparticles (NPs) with a maghemite (γ-Fe_2O_3) core of 7 nm, synthesized by coprecipitation.[29] These nanoparticles possess superparamagnetic properties detailed elsewhere,[30] which make them suitable for both MRI and heat generation. Their biodistribution and biotransformation were previously characterized, showing degradation over three months and iron recycling into ferritin.[17,21] These particles are currently developed by Guerbet SA as a new T2 clinical contrast agent for imaging inflammation processes.[12,13,15,31] In this study we investigated the role of three different surface coatings in particle interactions with plasma. The so-called Pi903 NPs are raw negatively charged platforms provided with carboxylic moieties on the particles' surface. P904 NPs have been derived from Pi903 precursors by functionalization of carboxyl functional groups with an amino-alcohol derivative of glucose. These particles were designed to minimize interactions with plasma proteins. Their zeta potential is strongly reduced compared to Pi903 (ξ-potential of −37.4 mM *versus* −52 mV for Pi903). Citrate-coated NPs (ξ-potential of −31.6 mV) were also used for comparison. All NPs behave as magnetic monodomains and show comparable magnetic size distribution, superparamagnetic properties, and colloidal stability in aqueous suspension (see Supporting Information Figures 1S and 2S). All physicochemical characterizations of bare nanoparticles are summarized in Table 1.

***In Situ* Quantification of the Adsorption of Macromolecules on Nanoparticles by Dynamical Magnetically-Induced Birefringence Method.** The adsorption of proteins on magnetic nanoparticles was quantitatively monitored *in situ* by a magnetically induced optical birefringence experiment. This technique measures the optical birefringence

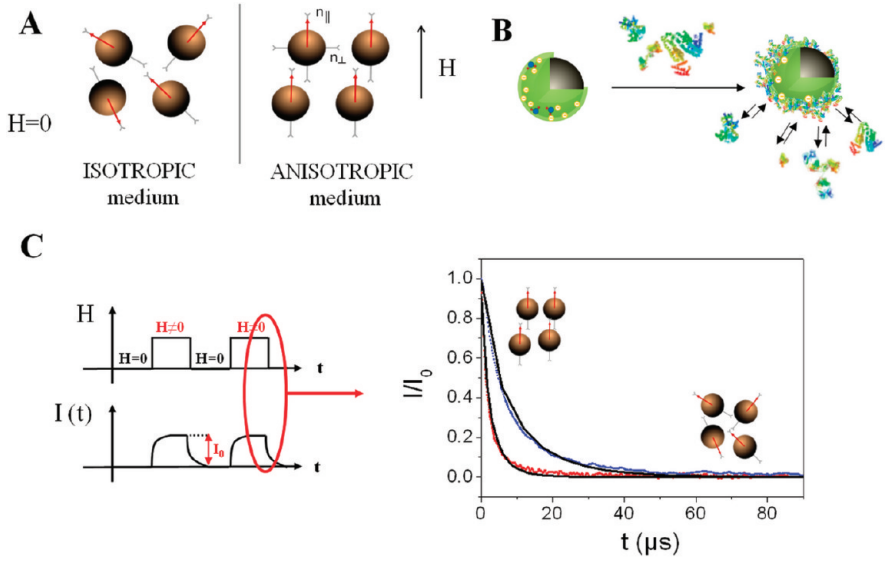

Figure 1. (A) Schematic representation of the orientation of nanoparticle magnetic moments (red arrows) and optical axes (gray arrows) in the absence (left) or presence (right) of an external magnetic field. (B) Interactions between nanoparticles and blood proteins in biological media. (C) A pulsed magnetic field is applied to the suspension of nanoparticles and the time-dependent birefringence signal $I(t) \propto n_{\parallel} - n_{\perp}$ is recorded. The relaxation of birefringence signal $I(t)$ after switch off of the field fits a *stretched-exponential* law (black line) and is slackened for BSA−NP complexes (blue dots) compared to the bare NPs (red dots).

signal provided by an assembly of magnetic nanoparticles in suspension, when they are magnetized by a static magnetic field. The coupling between the directions of magnetic moment and optical axis of a monodomain nanoparticle is ensured by both shape and magnetocrystalline anisotropies of the ferrimagnetic lattice constituting the nanocrystal.[32] Therefore the orientational distribution of the nanoparticles' optical axes follows the dynamics of their individual magnetic moments in response to the externally applied magnetic field (Figure 1A). Conversely, when the magnetic field is switched off, the birefringence relaxes to zero together with the magnetization of the sample. This relaxation is directly related to the orientational Brownian motion of the nanoparticles, which lose their field-induced orientation.[33] Following the Stokes−Einstein equation, the hydrodynamic volume V_H of the rotating complex can be deduced from the orientational relaxation time $\tau = 3\eta V_H/k_BT$ assuming a spherical shape of the rotating complexes, where η is the viscosity of the carrier fluid, T the temperature, and k_B the Boltzmann constant.

This measurement can be performed at any time in the same suspension which is thermalized at 37 °C, allowing real time monitoring of the hydrodynamic size of the NP complex interacting or not with macromolecules (Figure 1B). Figure 1C displays typical birefringence signal decay after the magnetic field has been switched off (note that the switch-off of the field lasts less than 250 ns, which is much shorter than the relaxation time of the birefringence). The relaxation of birefringence is clearly slowed down in the presence of albumin or plasma. Thus we directly observe in real time the increase of the nanoparticle hydrodynamic size due to protein binding.[33]

Quantitatively, the decay of the magnetically induced birefringence signal is nonexponential but can be well fitted by a stretched exponential function as representation of relaxation time distribution, $I(t) = I_0 \exp[-(t/\tau_0)^{\alpha}]$. Here, I_0 is the equilibrium birefringence signal upon exposure to a 100 G magnetic field, τ_0 is the characteristic relaxation time constant, and α ($0 < \alpha < 1$) is the stretching exponent, controlling the width of the relaxation time distribution (the smaller α is, the wider is the distribution).

Conversely, from the stretching exponent α and characteristic time τ_0, we can extract a probability density $P(R_H)$ for a particle's hydrodynamic radius R_H, approximated by

$$P(R_H) = \frac{3}{2R}\alpha\left(\frac{R_H}{R_0}\right)^{\alpha} \exp\left[-\left(\frac{R_H}{R_0}\right)\right] \qquad (5)$$

Unlike a dynamic light scattering experiment, the birefringence method detects only the nanoscale change related to magnetic NPs. Owing to this specificity, the measurement is not perturbed by light diffusion of plasma proteins, including aggregates, and can be performed *in situ* and in real time even in pure plasma. Thus this method avoids separation processes that eliminate excess protein, which often compromise the integrity of the protein corona on the nanoparticles. Being sensitive to less than one nanometer change in protein corona thickness, it makes it possible to distinguish even tiny variations in the protein corona from NP's aggregation process. Moreover, unlike fluorescence correlation microscopy, a method which was recently proposed for quantification of protein layers on nanoparticles,[25] this magneto-optical method does not require a fluorescent

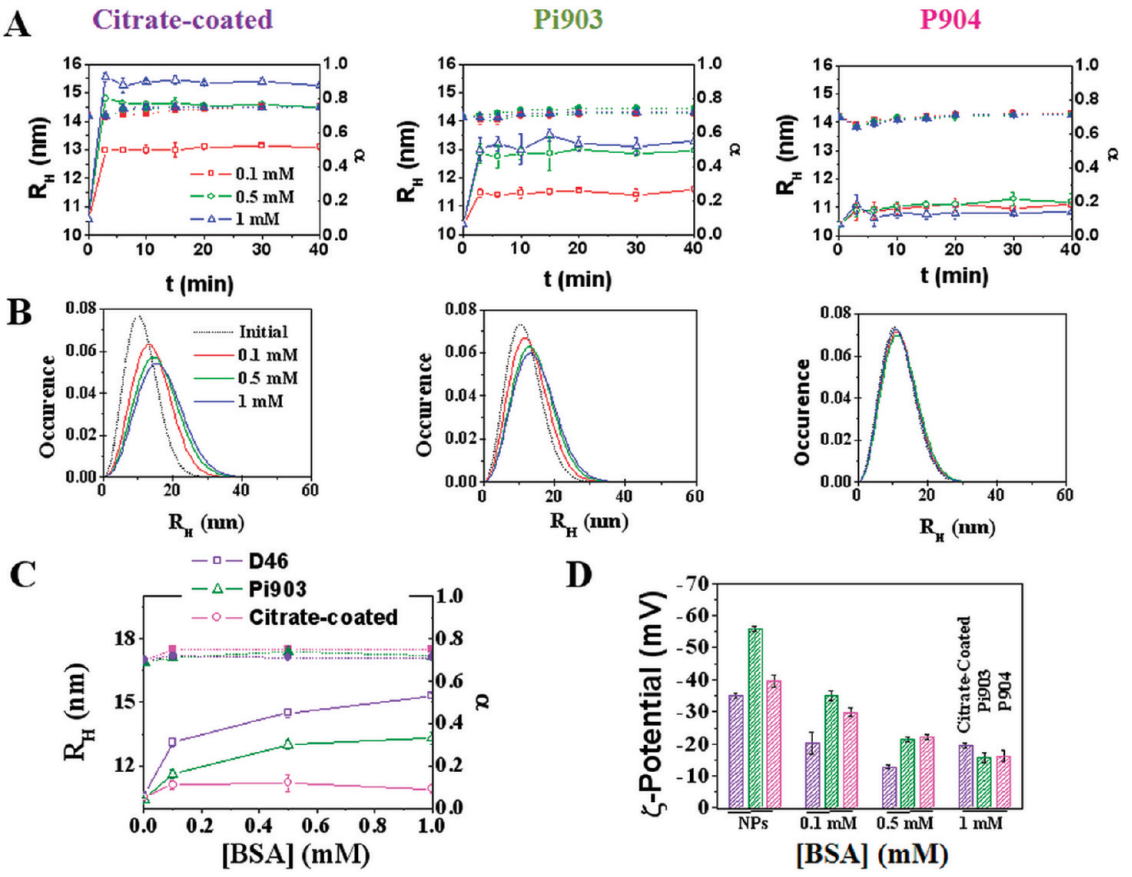

Figure 2. Interactions of NPs with BSA probed by magnetically induced birefringence. (A) Mean hydrodynamic radius (open symbol) and stretching exponent (solid symbol) as a function of time with BSA at different concentrations, (B) Hydrodynamic radius distribution after 40 min of incubation with BSA compared to the initial bare NP distribution. BSA concentration-dependence of the mean hydrodynamic radius and stretching exponent (C), and ξ-potential (D) after 40 min of incubation. The data points were averaged from three independent measurements.

marker, which may eventually interfere with plasma protein adsorption on the nanoparticle surface.

Interactions of Iron Oxide Nanoparticles with Albumin. When dispersed in aqueous suspensions, P904, Pi903 and citrate-coated NPs show a characteristic relaxation time of τ_0 = 2.18, 2.14, and 2.62 μs and a stretching exponent of α = 0.70, 0.69, and 0.70, respectively. This stretching exponent value (around 0.7) is representative of the intrinsic distribution of the hydrodynamic size of the nanoparticles (correlated with crystalline and magnetic size distributions, see Supporting Information Figures 1S and 2S), and reveals the absence of aggregated nanoparticles in the suspension. As a first model protein, we selected albumin, the most abundant protein in plasma (about 55% of total plasma proteins, corresponding to a plasmatic concentration of 0.5 to 0.8 mM). Serum albumin is a prism-shaped α-structure protein of dimensions 8 × 8 × 3.8 nm and a molecular weight of 67 kDa.[34] The nanoparticles were incubated at 37 °C in deionized water with increasing concentrations of bovine serum albumin (BSA) ([BSA] = 0.1, 0.5, and 1 mM for a final iron concentration [Fe] = 10 mM, corresponding to 70, 330, and 660 BSA molecules per nanoparticle, respectively). After the addition of albumin, the fits of the birefringence decay typically yield an increase in τ_0 (Figure 1C). Interestingly the change in the birefringence relaxation dynamics occurs in less than 2 min following the contact of nanoparticles with proteins and reaches equilibrium from 10 min (Figure 2A). A slight decrease in the stretching index α is observed in the first 10 min and then the value increases again to stabilize at a value slightly greater than that observed initially in the absence of proteins. This shows that the system passes through a short-lived regime of instability in the first minutes before reaching equilibrium. However we observed some differences in the hydrodynamic radius distribution depending on the nanoparticle surface state and on BSA concentration (Figure 2B). There was very little change in the hydrodynamic size of P904, demonstrating none or very poor interaction with BSA (average radius increment ΔR_H = 0.7 ± 0.2, 0.8 ± 0.4, and 0.4 ± 0.2 nm for 0.1, 0.5, or 1 mM BSA concentration, respectively). In contrast, the hydrodynamic radius of Pi903 and citrate-coated NPs increases of 3.0 ± 0.3 nm and 4.7 ± 0.2 nm, respectively, reflecting a dose-dependent albumin adsorption on the nanoparticle surface. In the case of Pi903, this increase leveled off for an albumin concentration of

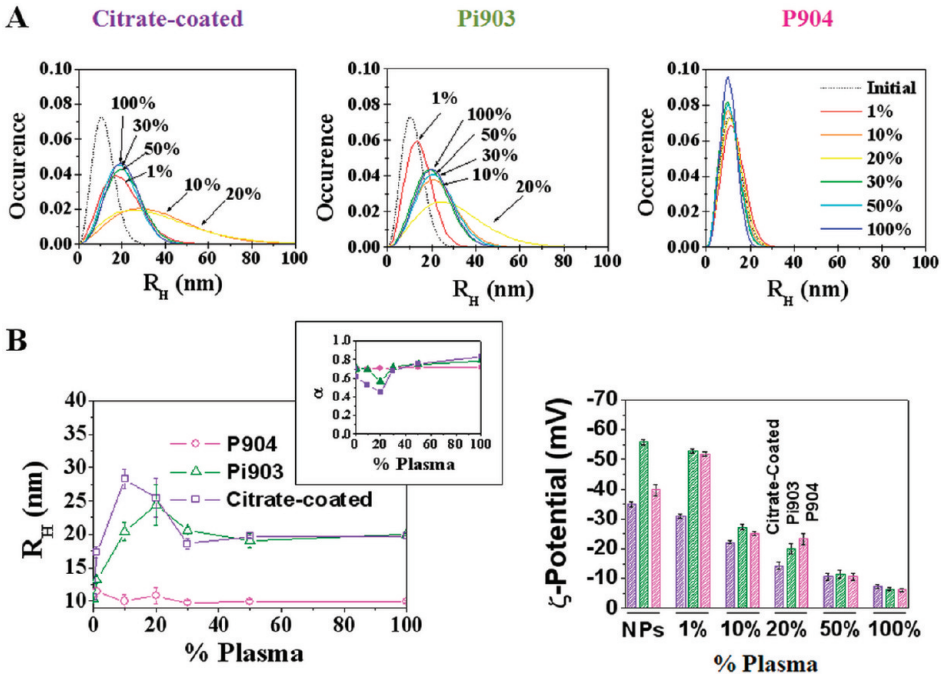

Figure 3. Interactions of NPs with blood plasma probed by magnetically induced birefringence. (A) Hydrodynamic radius distribution after 40 min of incubation with plasma at different dilutions. Plasma dilution dependence of the mean hydrodynamic radius (B), stretching exponent (inset B), and ξ-potential (C) after 40 min of incubation. The data points were averaged from three independent measurements.

0.5 mM with a protein layer thickness that is in line with the values reported in the literature for a monolayer of albumin (Figure 2C).[25] The relationship proposed by Röcker *et al.*,[25] $R_H(N) = R_H(0) = (1 + cN)^{1/3}$ (where $R_H(0) = 10.4$ nm and $c = V_P/V_0 = 0.021$ for Pi903), yields a number N of adsorbed proteins. The maximum number of bound proteins was found around 50 per Pi903 NP and 10 for P904, whereas a total of 330 albumin molecules was available in solution.

On citrate-coated NPs, BSA adsorption resulted in an increasing hydrodynamic size which did not saturate for [BSA] = 1 mM. This finding suggests a conformation of albumin molecules on the surface of citrate-coated NPs, which is different to that on Pi903 surface. Interestingly, in all cases, the slight enhancement of stretching exponent reveals a homogenization of the particle size due to albumin coating which tends to better stabilize the nanoparticle suspension.[28] Simultaneously, the zeta potential (reflecting the charge measured at the NP surface including the associated counterions) also changed to lower absolute values, diminishing the differences of the initial NP surface (Figure 2D).

Interactions of Iron Oxide Nanoparticles with Plasma Proteins Depend on Plasma Concentration. After studying the interactions of NPs with albumin, the most abundant plasma protein, we investigated the effect of whole blood rat plasma, which contained several thousand different proteins in different concentrations, competing for binding to the surface of the NPs. NPs ([Fe] = 10 mM) were incubated in a water suspension with increasing concentrations of plasma (1%, 10%, 20%, 30%, 50%, and 100%). Typically the 10% plasma suspension is representative of the culture medium used for cell culture *in vitro,* while the 100% plasma suspension is characteristic of the *in vivo* situation in which NPs are directly injected into the bloodstream.

As observed in the case of albumin, the kinetics of protein layer formation were very fast for the three samples (see Supporting Information Figure 3S), occurring in less than 2 min. A stable relaxation time was then found during the 40 min incubation. The characteristic hydrodynamic radius R_{H0} and stretching exponent α are plotted in Figure 3B as a function of plasma concentration after 40 min of incubation, together with the hydrodynamic size distribution $P(R_H)$ of the different samples (Figure 3A). Surprisingly, their dependencies on plasma concentrations were not monotonous. For Pi903 and citrate-coated NPs, the stretching exponent α first decreases at low plasma concentration and starts to increase beyond 30% plasma concentration. Similarly, the average size starts to increase dramatically and then decreases to reach a plateau value after 50% of plasma. These data provide evidence of a destabilization of the colloid in 10% and 20% of plasma for citrate-coated NPs and in 20% of plasma for Pi903, which leads to the formation of stable clusters. Conversely, the stretching exponent retrieves its initial value beyond 50% of plasma, showing that no aggregation occurs at higher concentration of plasma. Meanwhile the equilibrium size is shifted toward a higher value in suspensions with high plasma concentration,

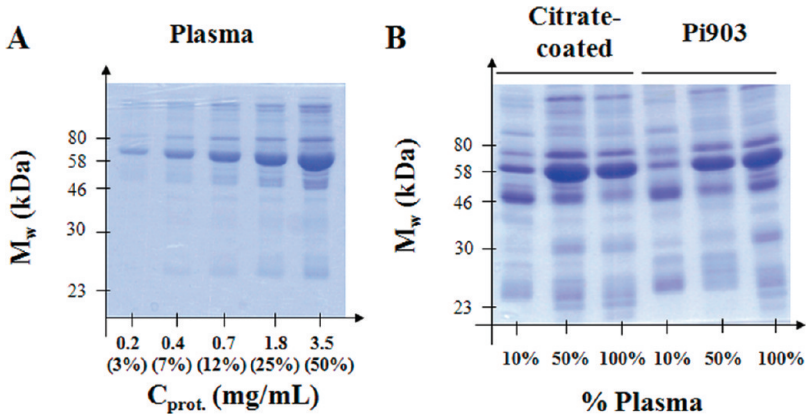

Figure 4. SDS-PAGE and Coomassie Brilliant Blue staining of plasma proteins at different dilutions (A), and of proteins absorbed on nanoparticles (B) after 40 min incubation with plasma solution.

showing the formation of a stable protein corona with a thickness of ΔR_H = 8.8 nm, almost similar for both Pi903 (8.8 ± 0.5 nm) and citrate-coated NPs (8.8 ± 0.2 nm).

This difference in particle behavior in different plasma concentrations suggests that the nature of the protein corona may vary. At low plasma concentration, the interactions with some of the most abundant proteins may cause particle clustering. In contrast, at higher concentration, the proteins causing aggregation may be displaced by other proteins, which are less abundant but show a greater affinity for the nanoparticles and tend to stabilize them as isolated ones with a protein corona of 8.8 nm thickness. It is worth noting that albumin alone did not produce such an enhancement of hydrodynamic volume in any of the samples. Remarkably, in the case of P904 NPs, size distribution remained unchanged regardless of the plasma concentration. This demonstrates that the glucose derivative coating of P904 NPs is very efficient in inhibiting plasma protein adsorption compared to the noncoated Pi903 precursor. In contrast, Pi903 and citrate-coated NPs exhibit competitive binding processes and concurrent exchange with free proteins in plasma, resulting in drastically different behaviors as one passes from plasma concentrations used for *in vitro* cell studies to those present *in vivo*.

Qualitative Comparison of Adsorbed Proteins on Nanoparticles by Gel Electrophoresis. To elucidate the nature of the protein corona as a function of plasma concentration, sodium dodecyl sulfate-polyacrylamide gel electrophoresis (SDS-PAGE) was carried out (Figure 4). The most common method used to separate nanoparticles with their protein corona from excess plasma is centrifugation. However, centrifugation can become inappropriate for small diameter colloidal NPs, as it can induce the precipitation of some protein aggregates together with NPs or disrupt some weakly bound protein−particle complexes. Here, we took advantages of the NPs' superparamagnetic properties to separate them by an external magnetic field gradient. As the magnetic birefringence method specifically monitors the hydrodynamic volume of magnetic NPs, this separation method first introduced by Mahmoudi *et al.*[24] increases the specificity of NP isolation. According to the colloidal stability of the nanoparticles, the suspension was magnetically decanted for 1 h to 2 days until quasi-complete separation. The supernatant was removed and the precipitate was washed three times in the presence of the magnet to remove excess plasma before analysis by gel electrophoresis. Figure 4B illustrates SDS-PAGE of Pi903 and citrate-coated NPs incubated for 1 h in plasma concentration from 10% to 100% (SDS-PAGE of initial bare NPs are shown in Figure 4S (Supporting Information)). For comparison, the SDS-PAGE of pure plasma with increasing concentrations is also displayed, showing the expected increase in intensity of typical bands (Figure 4A). However, in the case of Pi903 and citrate-coated NPs that were analyzed at constant iron concentration, all observed bands did not increase with the incubated plasma concentration. Some bands (*e.g.*, at 50−70 kDa molecular weight, M_w) show decreasing intensity with increasing plasma concentration, whereas others (*e.g.*, at 28 kDa) only appear for high plasma concentrations. Overall, the same experiment carried out in three independent replicates gives evidence that the protein pattern changes significantly with increasing plasma concentration. In line with the evolution of the hydrodynamic size derived from magnetic birefringence measurements, protein fingerprints suggest that the destabilizing proteins linking nanoparticles at low plasma concentration are partially or fully desorbed at higher plasma concentrations by competitive proteins with higher binding affinity, surface coverage of the nanoparticle, and subsequent stabilizing effect. The fact that protein patterns are rather similar for citrate-coated and Pi903 NPs is also in agreement with the identical protein corona thickness of 8.8 nm found for both NPs. Although some subtle differences can exist in the kinetics of protein adsorption, Pi903 and citrate-coated NPs show similar behaviors with respect to the plasma concentration, while P904 NPs do not adsorb proteins as confirmed by SDS-PAGE.

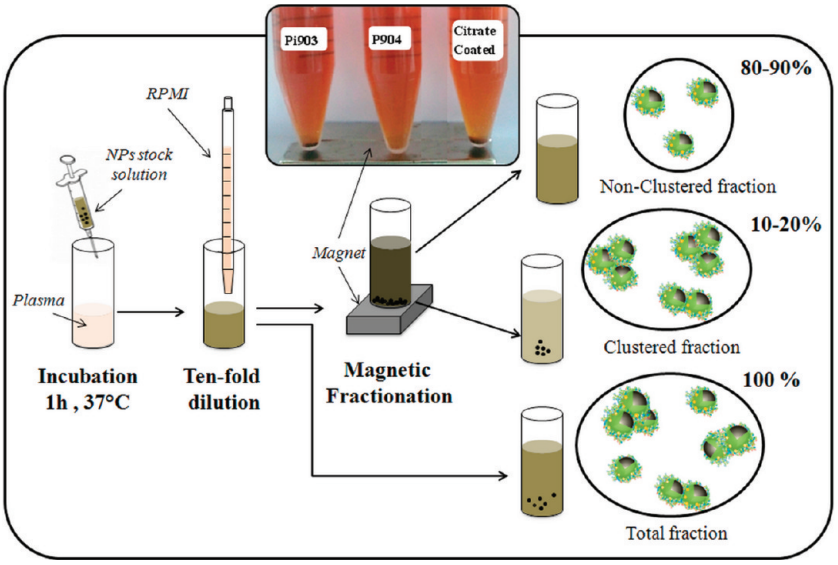

Figure 5. Schematic diagram for magnetic fractionation of protein/NP complexes. NPs are first incubated for 1 h in whole plasma, then diluted 10-fold in RPMI culture medium (total fraction). Upon application of the magnet for 2 min, the fraction containing clustered NPs (clustered fraction representing 10−20% of the total fraction) is separated from the supernatant containing nonclustered NPs (nonclustered fraction).

The reported findings concerning the evolution of protein corona with plasma concentration is rather unusual for nanoparticles, since it has been generally reported that more proteins of the same type bind in function of increasing plasma concentration.[35] However the Vroman effect, applied on macroscale surfaces, describes how proteins can be displaced by others with higher affinity for the surface, depending on the available surface area and diffusion coefficient of proteins.[36] For nanoscale particles displaying high surface curvature and high surface area, the formation and exchange of the corona may be due to the interplay of various phenomena, depending on size,[3,37] surface charge,[3] surface roughness,[38] or hydrophobicity.[35] In line with present results, it was recently reported that silica nanoparticles of 50 and 200 nm presented a protein corona that exhibited decreasing thickness when plasma concentration was increasing and whose composition varied, especially between 20% and 40% plasma concentration.[35] Moreover there was some evidence for clustering of NP-protein complexes at low plasma concentration. Mass spectrometry (MS) analysis identified a decrease in the intensity of the SDS-PAGE protein bands at 50−70 kDa due to the decrease of the fibrinogen content with increasing plasma concentration, while other abundant proteins like albumin were enhanced.[39−41] In a similar way, we observed here a significant decrease in the 50−70 kDa band, likely corresponding to fibrinogen and the enhancement of the 28 kDa band corresponding to apolipoprotein A-1.[40] Although we do not quantitatively analyze the whole range of proteins adsorbed on particles, our qualitative results suggest that fibrinogen plays a role in the aggregation of Pi903 and citrate-coated NPs at low plasma concentration while other proteins, such as apolipoproteins, tend to stabilize single nanoparticles at higher plasma concentration.

The Cell Perceives Different Populations of Nanoparticles with Distinct Biological Identity and Aggregation State. In the above-described analysis, we emphasize the differences in what the cell should perceive in regard to iron oxide nanoparticles administrated *in vitro* (at low plasma concentration) or *in vivo* (high protein concentration in the blood). The uptake of nanoparticles by the monocyte−macrophage system is still not fully understood, mainly because conditions *in vitro* do not reproduce all complex *in vivo* nanobio-interactions.[6] Several hypotheses state that macrophage uptake of NPs results from the interplay of the nature of the protein corona, its effect on cell surface receptors, aggregation of nanoparticles triggering different cell responses and the combined/interconnected effect of NPs and protein clustering.[35,42−44] According to the results reported above, a preincubation in the whole plasma is mandatory to obtain NPs with the closest biological identity to the one achieved *in vivo* in the bloodstream. Therefore we proposed the following protocol for cell uptake assay. Pi903, P904, and citrate-coated NPs were first incubated in rat plasma (100%) for 1 h at 37 °C. The NP-plasma mixture was then diluted to one-tenth in RPMI culture medium in order to obtain a medium ([Fe] = 10 mM, 10% serum), which is suitable for *in vitro* incubation with macrophages. An important issue, which was never addressed, is to evaluate whether cells perceive a homogeneous population of nanoparticles or if the intricate interactions of NPs with the myriad of plasma proteins result in different populations of nanoparticles

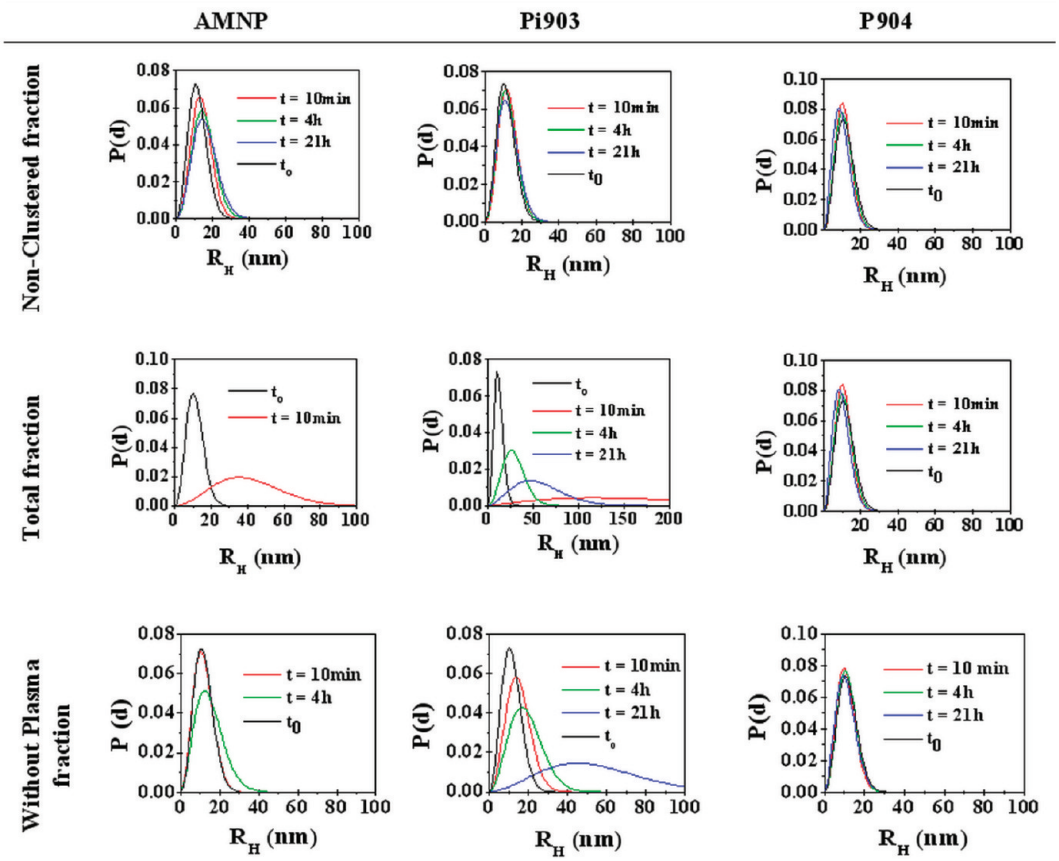

Figure 6. Time evolution of the size distribution of different NP fractions in RPMI medium. Data points were averaged from three independent measurements.

with distinct biological identities and apparent sizes. To shed light on this issue, we used magnetic fractionation to separate different populations of protein−nanoparticle complexes based on their magnetization. This method allows isolating NP clusters with large magnetization from individual NPs. We then characterized the hydrodynamic size, iron content, protein fingerprints, and macrophage uptake of each fraction. Immediately after dilution in RPMI medium, the suspension was exposed to an external magnet for 2−3 min. The magnet did not affect the stability of the P904 suspension, but in the case of Pi903 and citrate-coated NPs solutions, a small fraction of NPs (called the "clustered" fraction) was attracted by the magnet, while the majority of NPs remained in solution forming the so-called "nonclustered" fraction (Figure 5). In contrast to the previous separation protocol (for SDS-PAGE characterization), the magnet was applied for a short time. Consequently only clustered nanoparticles underwent a sufficient magnetic force and were attracted to the magnet.

The "clustered" and "nonclustered" fractions (suspended in the same volume of RPMI) were then analyzed over time by magnetic-optical birefringence (Figure 6, see also Supporting Information available Table 1S) in comparison to the same NPs prior to magnetic fractionation ("total fraction") or without preincubation with plasma ("without plasma" fraction). We first noticed that NP aggregation in clustered fractions causes a high diffusivity of the solution that prevented any birefringence measurement. In contrast, the nonclustered fractions (corresponding to 80% and 100% of the initial amount of Pi903 and P904 NPs) kept their remarkable stability over time, presenting unchanged hydrodynamic size distribution after 10 min, 4 h, or 21 h in culture medium. The nonclustered fraction of citrate-coated NPs (60% of the initial amount) was also stable over time, with a slight evolution of the protein corona thickness from 4.7 to 7.2 nm. Consistently with the results reported above, there was no detectable protein corona on P904 NPs, while a 2.5 nm corona was bound to the Pi903 precursors. However the most remarkable result was that the nature of proteins bound to the nanoparticles was different in the clustered and nonclustered fractions as revealed by gel electrophoresis (see Supporting Information Figure 5S). Fibrinogen and albumin were most prominent in clustered fractions, whereas they were hardly detectable in the nonclustered ones. In contrast, apolipoprotein was enhanced in the stable fractions of citrate-coated NPs, confirming its stabilizing role. Although subtle variations of the protein patterns were observed depending on the original NP surface state, the same tendencies were found for citrate-coated NPs and enabled distinguishing

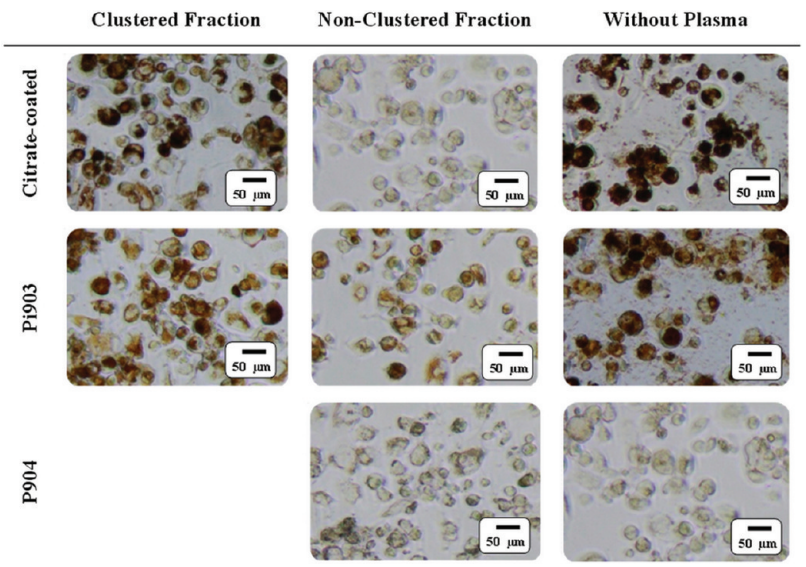

Figure 7. Bright field microscopy panels of macrophages incubated for 21 h with the clustered fraction and nonclustered fraction resulting from preincubation in pure plasma and with total fraction without preincubation in plasma.

the proteins embedded in NP aggregates from those coating single particles, ensuring their colloidal stability. Altogether, these findings highlight the heterogeneous nature of protein corona and its aggregation state among the nanoparticles exposed to plasma, with the exception of P904 NPs, which display a single stable population. In line with results on separated fractions, the total fraction exhibited a larger mean hydrodynamic size than the nonclustered fraction, reflecting the presence of aggregates at $t = 0$. The destabilization of the total fraction was observed over time in RPMI medium for Pi903 NPs and, in a faster way, for citrate-coated NPs, whereas P904 remained stable up to 21 h. Interestingly, NP flocculation also occurred in RPMI medium alone without previous incubation in 100% plasma. In contrast, with or without preincubation in plasma, all three types of NPs remained stable over time for up to 21 h when diluted in water instead of RPMI culture medium (see Supporting Information Table 2S). This indicates the nontrivial relationship between protein adsorption (triggered by interactions with plasma proteins) and the aggregation effect, which does not necessarily involve proteins alone. Therefore it becomes important to distinguish different phenomena: protein adsorption on isolated NPs showing a stabilizing effect, protein-induced clustering of NPs, and protein-free aggregation effect, which may all result in different cell response.

Uptake of Nanoparticles by Macrophages: Role of Protein Adsorption and Colloidal Stability. To investigate the interactions of NPs with macrophages, we used the human monocyte THP1 cell line, which was activated into macrophages by treatment with a phorbol ester. The so-obtained adherent macrophages were incubated for 21 h at 37 °C with different fractions of NPs in RPMI medium, namely the clustered and nonclustered fractions after preincubation in pure plasma or the nanoparticles without preincubation in plasma. Cellular uptake of NPs was quantified by single cell magnetophoresis which consists in measuring the velocity of a magnetically labeled cell in a well-defined magnetic field gradient.[45] This magnetic method allows measurements on individual cells and gets rid of nanoparticles or aggregates which are not bound to the cell.[46] For comparison, total iron quantification by flame atomic spectrometry was performed in a pellet of macrophages after rinsing and centrifugation. The last dosage quantifies NP flocculates in addition to the cell-associated NPs.

As expected from the above-mentioned magnetic birefringence follow-up, both the clustered fraction and without-plasma fraction of citrate-coated and Pi903 NPs showed a visual agglomeration on cells after 21 h incubation (Figure 7). To the opposite, the nonclustered fraction of citrate-coated and Pi903 NPs and all the fractions of P904 NPs remained in suspension during their incubation with macrophages, with no trace of NP flocculates either on the cells or on the surface of the culture dish. As a consequence, the iron load per cell determined by single cell magnetophoresis was very close to the value derived from total iron dosage (Table 2). In contrast, the destabilization of the colloid in the flocculated and "without plasma" fractions resulted in a total iron amount which was 2 to 5-fold higher than the actual iron load per cell.

The role of particle aggregation and protein coating on cell uptake was revealed by the comparison of the absolute iron load per cell determined by magnetophoresis. Aggregated NPs were efficiently uptaken by macrophages, leading to an iron load of up to 48 pg per cell. Cell capture was significantly enhanced for protein-associated NP clusters (clustered fraction, 48.8 and 39.2 pg/cell for citrate-coated and Pi903 NPs, respectively) when compared to aggregates formed in RPMI

TABLE 2. Iron Concentration in Macrophage Incubation Medium and Iron Load Per Macrophage after 21h Incubation with Different NP Fractions. Data Points Were Averaged from Three Independent Measurements

		iron load per cell after 21 h incubation (pg_{Fe}/cell)	
	iron concentration in incubation medium [Fe] (mM)	single cell magnetophoresis[a]	iron assay (flame)
	citrate-coated		
without plasma fraction	10	41.0 (0.8)	104.1
total fraction	10		
non-clustered fraction	6	18.8 (0.6)	15.6
clustered fraction	2	48.8 (0.6)	157.4
	Pi903		
without plasma fraction	10	31.6 (0.8)	148.9
total fraction	10		
non-clustered fraction	8	30.7 (0.6)	49.1
clustered fraction	1	39.2 (0.5)	102.1
	P904		
without plasma fraction	10	5.6 (0.8)	1.9
total fraction	10	6.1 (0.6)	4.1

[a] Iron load per cell determined by single cell magnetophoresis is expressed as mean iron load m (pg_{Fe}) with relative standard deviation $\Delta m/m$ in brackets.

medium alone without preincubation in plasma (41.0 and 31.6 pg/cell, respectively). Protein coating on individual nanoparticles (nonclustered fraction) also resulted in a high degree of cell association (18.8 and 30.7 pg/cell, for citrate-coated and Pi903 NPs, respectively) despite the fact that cells perceive individual nanoparticles dispersed in the culture medium rather than clusters tending to sediment on their surface. The slightly different protein profiles on citrate-coated and Pi903 NPs (see Supporting Information Figure 5S) could likely explain the observed differences in cell uptake.

Conversely, the uptake of P904 nanoparticles remained rather low (<7 pg/cell), regardless whether they have been preincubated in whole plasma or not. Their glucose-derivative coating prevents both adsorption of plasma proteins (irrespective of the protein type) and rapid capture by macrophages. This suggests that for such a coating, the identity of NPs injected *in vivo* could be close to that obtained *in vitro*. Minimal interactions with proteins in conjunction with the absence of aggregation could account for the observed long circulation time of P904 NPs injected *in vivo*. In line with presented results, these NPs have been shown to be appropriate to target circulating monocytes or peripheral macrophages involved in inflammatory processes, before being fully cleared by the first "filter"—the resident macrophages of the liver and spleen.[12,13,15,31] Thereby our findings suggests that protein adsorption is not the main trigger for macrophage uptake of P904 NPs, but kinetic parameters likely govern the distribution of these NPs among different cell subsets in the organism.

The scheme appears quite different for the citrate-coated and Pi903 precursors, which present different profiles to cells due to their interactions with plasma. We evidenced for the first time that cells can simultaneously face very dissimilar populations of NPs in regard to their association with proteins and/or the nature of the latter, and to their level of aggregation. Moreover such heterogeneity also translates to cell uptake capacity. While our approach tried to mimic at least some of the complex *in vivo* conditions (obtained by preincubation with the whole plasma), we hypothesize that the plurality of NP behaviors can also be found in the organism and can be predictive of their biological outcomes. In the light of our results, it could be predicted that the protein-stabilized nanoparticles (corresponding to the nonclustered fraction) would circulate in the bloodstream for a longer time than the NP-protein clusters, mainly "decorated with" opsonins like fibrinogen – which will, in turn, promote phagocytosis and removal from the circulation by the mononuclear phagocytic system of the liver and spleen. Moreover, the protein-stabilized nanoparticles could partly escape the resident macrophages and preferentially interact with peripheral macrophages involved in tissue homeostasis. In particular, apolipoproteins are expected to affect the NP distribution, depending on the pathophysiological conditions.[6,47] Here again, the kinetic issue will likely play a key role in governing the biodistribution and fate of different subsets of NP–protein complexes and requires further consideration. From the present results, we can infer that the interactions of NPs with plasma proteins occur faster than their associations with cells, as previously reported.[35,43,48] The biological identity of nanoparticles, although being plural, does not evolve substantially after the first hour of exposure in plasma. Remarkably, the protein-stabilized nanoparticles as well as P904 NPs did not change their status up to 21 h. The aggregation process, although accentuated with time, occurs early after exposure to plasma. Thus the kinetic control of macrophage uptake might be mainly governed by cell interactions with the preformed protein–NP complexes, depending on their size, their charge, and protein content. Owing to the magnetic fractionation of distinct complex populations, we provided evidence of the differences in cell uptake resulting from distinct protein content and aggregation state. Whereas previous studies suggested that cell uptake was correlated with the amount

of proteins bound in the NP corona,[42,43] we show here that the heterogeneity in biological and physical identity of NP−protein complexes also determines their biological fate.

CONCLUSIONS

The contribution of this study is 2-fold, both methodological and conceptual. First, we developed novel accurate methods based on nanomagnetism to specifically address the interactions of proteins with magnetic nanoparticles and their subsequent effect on cell uptake. The tracking of nanoparticle orientation by the magnetically induced dynamic birefringence method provides a real time, sensitive, and quantitative *in situ* detection of protein corona on particle surface. As little as one nanometer variations in the thickness of protein corona could be measured in plasma medium. Coupled to magnetic separation or the fractionation technique, this method makes it possible to distinguish the dynamic processes leading to the coating of individual nanoparticles by proteins or to the onset of NP aggregation, whether or not mediated by proteins. The specificity of magnetism-based methods enhances the reliability of *in situ* results by getting rid of artifacts due to free proteins. Moreover these methods do not require centrifugation steps, which may affect the NP/protein complexes. Magnetic fractionation also enables the separation of different populations of NP complexes according to their clustering level and reveals the differences in protein fingerprints. Single cell magnetophoresis also specifically quantifies macrophage uptake of magnetic nanoparticles, without interfering with NPs that are not strongly bound or internalized by the cell.

The reported results further contribute to delineate the intricate effects of plasma proteins on nanoparticles with a given size (8 nm core), surface curvature, and chemical composition, but with different surface chemistry. The hydrophilic glucose-derivative coating of P904 NPs successfully inhibits protein adsorption on their surface and enables both high stability in biological media and low uptake by macrophages. By contrast the bare and more negatively charged surface of Pi903 or citrate-coated NPs favors highly complex interactions with blood plasma proteins, which have been quantified in this study. An important result, with high impact on the extrapolation of *in vitro* to *in vivo* behavior of NPs, is that these interactions depend on the concentration of available plasma proteins. At low plasma concentrations (representative in mostly used *in vitro* conditions), NPs tend to form clusters triggered by proteins like fibrinogen, whereas at high plasma concentration (closer to physiological situation) other proteins such as apolipoproteins tend to coat and subsequently stabilize individual NPs. Moreover this plurality of NP behaviors, which coexists to a certain extent depending on the incubation conditions, significantly affects macrophage uptake. Thanks to magnetic fractionation, it is demonstrated that the cell perceives dissimilar populations of NPs which differ in their level of clustering, as well as in their protein fingerprint. Macrophage capture is shown to vary when a cell interacts with protein-stabilized individual NPs, protein-induced NP clusters, or protein-free NP aggregates. This suggests that for a single population of NPs administrated into the circulation, a variety of protein−NP complexes may be found in the bloodstream with distinct biological fates.

MATERIALS AND METHOD

Materials. Rat plasma EDTA-K2 was provided from JANVIER. Roswell Park Memorial Institute medium (RPMI-1640), trypsin solution, and all other reagents used for cell culture were purchased from PAA and used with no further purification. Bovine Serum Albumin (BSA), phenylmethanesulfonyl fluoride solution (PMSF), and *N*,*N*,*N*′,*N*′-tetramethylethylenediamine (Temed) were purchased from Sigma-Aldrich. Ultrapure 99.99% sodium dodecyl sulfate (SDS) was purchased from Euromedex.

Magnetic Nanoparticles. Magnetic cores of maghemite with a diameter of 7−8 nm, covered by different surface coatings, were used in this study. They were synthesized following a classic procedure, by the coprecipitation of ferric and ferrous ions in an alkaline medium,[29] and coated with specific ligands. Citrate-coated nanoparticles are mainly developed for *in vitro* cell labeling.[49] They are stabilized in water supplemented with 5 mM of sodium citrate. Electrostatic repulsions are provided by the negatively charged carboxylate ligands complexed on the nanoparticle surface. P904 is currently developed by Guerbet SA for MRI detection of macrophages involved in inflammatory diseases. P904 is coated with aminoalcohol derivatives of glucose *via* carboxylate functions; their colloidal stability is ensured with both negative surface charges and steric hindrance. Pi903 is the precursor of P904, which is electrostatically stabilized by the presence of strong negative charges on its surface.

Physical Characterization. Dynamic light scattering (DLS) and ξ-potential measurements were recorded by means of a Malvern zetasizer nanoZS using a He−Ne laser (633 nm) at 25 °C. DLS was used to determine the NP hydrodynamic diameter and their polydispersity index (PDI) in the medium. The Contin model was applied to obtain size data. The ξ-potential was determined by measuring the electrophoretic mobility of NPs, which was converted to ξ-potential using the Henry equation.

Samples for transmission electron microscopy (TEM) were prepared by depositing NPs on carbon-coated copper grids. The measurements were carried out with a JEOL JEM 1011 microscope (100 kV). A large number of nanoparticles (200−400) were counted in order to obtain a statistically sound distribution, which fit a Gaussian distribution.

The magnetization of the NP colloidal suspensions was measured by a SQUID MPMS magnetometer, as a function of the magnetic field at room temperature. The magnetization curves fit a Langevin function weighted by a log-normal distribution of magnetic diameter. Fit parameters yielded the characteristic magnetic diameter d_{magn} and polydispersity index σ of the log-normal distribution.

Incubation of NPs with BSA and Blood Plasma. Stock solutions of NPs (iron concentration of 1.56 M, 518 mM, and 256 mM for citrate-coated, P904 and Pi903, respectively) were diluted in deionized water containing different concentrations of bovine serum albumin ([BSA] = 0.1, 0.5, and 1 mM) at a final iron

concentration of [Fe] = 10 mM and incubated at 37 °C for 40 min in this medium. Alternatively, NPs (final iron concentration of [Fe] = 10 mM) were incubated in different dilutions of rat plasma in water from 1% to 100%.

Magneto-optical Birefringence. The change in hydrodynamic diameter caused by the formation of a protein layer or by the onset of aggregation was determined by means of a magnetically induced birefringence experiment which is described in detail elsewhere.[31] In the presence of an external magnetic field, the NP suspension acquires a birefringence Δn ($\Delta n = n_{\parallel} - n_{\perp}$, $n_{\parallel}$ and $n_{\perp}$ being the optical indexes, respectively, in the direction of the magnetic field and perpendicular to it), due to the alignment of optical axes of the nanoparticles along the field and the subsequent alignment of their optical anisotropy axes.[31] This birefringence induces a phase lag φ proportional to Δn. In the optical set up illustrated in the Supporting Information, Figure 6S, a He−Ne laser beam (λ = 632.9 nm) of weak power goes through a polarizer (P), a quarter wave plate ($\lambda/4$); the ferrofluid sample is submitted to a pulsed vertical magnetic field, and an analyzer (A). The transmitted light $I(t)$ is collected on the photodetector (PD) and transmitted to a computer (PC) *via* the oscilloscope (Osc.). The light intensity detected by the photodetector is proportional to sin φ and to φ in the limit of a small phase lag. In the presence of the magnetic field, the collected light intensity saturates at the value I_0. The pulsed magnetic field is equal to 100 G and the birefringence decay is averaged over a large number of pulses (typically 512, total time of measurement 20s). The whole setup is thermalized at 37 °C, allowing *in situ* real time monitoring of the hydrodynamic size of the nanoparticle complexes in water, in BSA solution, in plasma solution, or in RPMI medium.

Electrophoresis SDS-PAGE. The protein/NP complexes were isolated from the solution containing excess proteins by magnetic separation under a strong permanent magnet (creating a magnetic field of **B** = 650 mT, and a magnetic field gradient **gradB** = 55 T m^{-1} in the volume of the container). The magnet was applied for 1 h to 2 days, depending on the colloidal stability of the NP suspension (The longest exposure time was applied to P904 NPs due to their high stability in plasma or RPMI medium). NPs that precipitated on the magnet were rinsed three times with water in the presence of the magnet to eliminate excess proteins. The footprint of proteins bound to the nanoparticles was resolved SDS-PAGE. A 10 μL portion of a diluted solution of each sample (with fixed iron [Fe] = 20 mM) was eluted in 10% SDS-PAGE. Electrophoresis was carried out using a Mini Trans Blot (Bio-Rad) coupled with a Heatkit Regulated H.V. power supply at 120 V in TGS buffer. After electrophoresis, the protein gel was stained for 30 min in a Coomassie Brilliant Blue solution. The gel and the destaining solution in the presence of a Cozap Pad for Coomassie Blue removal (Sigma-Aldrich) were placed in a tray to reveal the protein footprint.

Preparation of Incubation Medium for Cell Uptake Assay. Stock solutions of nanoparticles (iron concentration equal to 1.56 M, 518 mM, and 256 mM for citrate-coated P904 and Pi903, respectively) were diluted in 100% plasma solution to obtain a 100 mM iron concentration in a volume of 0.5 mL. After 1 h of preincubation at 37 °C, this solution was diluted 10 times in RPMI culture medium and a permanent magnet (**B** = 650 mT, and **gradB** = 55 T·m^{-1}) was placed under the solution for 2 min. The supernatant was collected to give the nonclustered fraction; the precipitate was dispersed in 5 mL of RPMI to obtain the clustered fraction. The iron concentration in each fraction was measured by flame spectroscopy. In addition, the total fraction before magnetic fractionation ([Fe] = 10 mM in RPMI medium) was used for incubation with cells. For comparison, a suspension of NPs directly diluted in RPMI medium ([Fe] = 10 mM) was also used without preincubation in total plasma (without-plasma fraction). The hydrodynamic NP size in each above-mentioned fraction and in water was monitored over time (up to 21 h) by magnetically induced birefringence.

Cell Uptake Assay. Human monocyte THP1 cell line was cultured in suspension (from 0.2 to 1 million cells/mL) in RPMI 1640 medium containing 10% (v/v) fetal bovine serum supplemented with 2 mM L-glutamine and 100 U/mL penicillin−streptomycin at 37 °C in 5% CO_2. Upon a 6-day treatment with phorbol ester (PMA, 50 ng/mL), the THP1 cells adhered to cell culture flasks and differentiated into macrophages as described elsewhere.[46] Macrophages were then incubated for 21 h with citrate-coated, P904 and Pi903 NPs within clustered, nonclustered, or a total fraction suspension (resulting from 1 h preincubation in total plasma) or in a serum-free RPMI medium ("without plasma" fraction). After three rinsing steps with RPMI medium, cells were trypsinized, centrifuged at 1200 rpm for 5 min, and rinsed twice again with RPMI. Subsequently the total iron concentration in cell pellets (containing a known number of cells) was quantified by flame atomic absorption spectroscopy. For a more specific measurement of cell iron load, a single cell magnetophoresis assay was used as described elsewhere.[45] Briefly, the cell magnetic load was quantified by measuring the velocity of magnetically labeled cells in suspension when they were submitted to a magnetic field gradient. In the steady state regime, the magnetic driving force acting on cells is defined as $\mathbf{F}_m = N \times \mu \times$ **gradB**, where N is the number of cell-associated NPs, μ the NP magnetization in the applied magnetic field, **B** = 145 mT, and **gradB** = 17 T/m, the magnetic field gradient. This force is counterbalanced by the viscous force $\mathbf{F}_V = 3\pi \times \eta \times d_{macr} \times v_{macr}$, where d_{macr} is the macrophage diameter (macrophages in suspension are assimilated to spheres), v_{macr} is the macrophage velocity, and η is the viscosity of the carrier fluid. The cell's magnetic moment (or equivalently the iron mass per cell) is thus derived from the measured cell velocity and cell diameter. The magnetophoretic movement of cells toward the magnet was recorded by video-microscopy. For each condition of incubation, the velocity and diameter of about 200 cells were measured, yielding the distribution of iron load in the cell population. The iron load per cell was expressed as a mean ± (standard deviation for three independent experiments).

Conflict of Interest: The authors declare the following competing financial interest(s):As research scientists in the company that provided, in part, contrast media nanoparticles, Anne Dencausse and Cecile Factor declare a conflict of interest.

Acknowledgment. We acknowledge Christine Ménager (PECSA, UPMC, Paris France) and Guerbet for providing us with citrate-coated nanoparticles and P904/Pi903 nanoparticles, respectively. We are grateful to Sébastien Ballet and Caroline Robic for fruitful discussions, to Jelena Kolosnjaj-Tabi for proofreading, and to Aude Michel for technical assistance. This work has been supported by the European project Magnifyco (Contract NMP4-SL-2009-228622).

Supporting Information Available: Figures showing TEM micrographs and the first magnetization curve at room temperature of the different NP samples, the evolution of the NP hydrodynamic radius as a function of time in plasma solution at different concentration, the SDS-PAGE and Coomassie Brilliant Blue staining of different NP samples diluted in water, the SDS-PAGE and the Coomassie Brilliant Blue staining of proteins absorbed on NPs in clustered and nonclustered fractions, the scheme of the experimental magneto-optical device and tables listing the time evolution of the hydrodynamic radius and stretching exponent for the different NP fractions dispersed in RPMI medium and dispersed in water after 1 h preincubation in pure plasma or without preincubation in plasma. This material is available free of charge via the Internet at http://pubs.acs.org.

REFERENCES AND NOTES

1. Gref, R.; Luck, M.; Quellec, P.; Marchand, M.; Dellacherie, E.; Harnisch, S.; Blunk, T.; Muller, R. H. 'Stealth' Corona−Core Nanoparticles Surface Modified by Polyethylene Glycol (PEG): Influences of the Corona and of the Core Composition on Phagocytic Uptake and Plasma Protein Adsorption. *Colloids Surf., B* **2000**, *18*, 301–313.
2. Cedervall, T.; Lynch, I.; Lindman, S.; Berggard, T.; Thulin, E.; Nilsson, H.; Dawson, K. A.; Linse, S. Understanding the Nanoparticle−Protein Corona Using Methods To Quantify Exchange Rates and Affinities of Proteins for Nanoparticles. *Proc. Natl. Acad. Sci. U.S.A.* **2007**, *104*, 2050–2055.

3. Lundqvist, M.; Stigler, J.; Elia, G.; Lynch, I.; Cedervall, T.; Dawson, K. A. Nanoparticle Size and Surface Properties Determine the Protein Corona with Possible Implications for Biological Impacts. *Proc. Natl. Acad. Sci. U.S.A.* **2008**, *105*, 14265–14270.
4. Mahmoudi, M.; Lynch, I.; Ejtehadi, M. R.; Monopoli, M. P.; Bombelli, F. B.; Laurent, S. Protein−Nanoparticle Interactions: Opportunities and Challenges. *Chem. Rev.* **2011**, *111*, 5610–5637.
5. Lynch, I.; Salvati, A.; Dawson, K. A. Protein−Nanoparticle Interactions: What Does the Cell See? *Nat. Nanotechnol.* **2009**, *4*, 546–547.
6. Aggarwal, P.; Hall, J. B.; McLeland, C. B.; Dobrovolskaia, M. A.; McNeil, S. E. Nanoparticle Interaction with Plasma Proteins as It Relates to Particle Biodistribution, Biocompatibility, and Therapeutic Efficacy. *Adv. Drug Delivery Rev.* **2009**, *61*, 428–437.
7. Yoo, D.; Lee, J.-H.; Shin, T.-H.; Cheon, J. Theranostic Magnetic Nanoparticles. *Acc. Chem. Res.* **2011**, *44*, 863–874.
8. Tassa, C.; Shaw, S. Y.; Weissleder, R. Dextran-Coated Iron Oxide Nanoparticles: A Versatile Platform for Targeted Molecular Imaging, Molecular Diagnostics, and Therapy. *Acc. Chem. Res.* **2011**, *44*, 842–852.
9. Pankhurst, Q. A.; Thanh, N. K. T.; Jones, S. K.; Dobson, J. Progress in Applications of Magnetic Nanoparticles in Biomedicine. *J. Phys. D: Appl. Phys.* **2009**, *22*, 224001.
10. Beckmann, N.; Cannet, C.; Babin, A. L.; Ble, F. X.; Zurbruegg, S.; Kneuer, R.; Dousset, V. *In Vivo* Visualization of Macrophage Infiltration and Activity in Inflammation Using Magnetic Resonance Imaging. *Wiley Interdiscip Rev: Nanomed. Nanobiotechnol.* **2009**, *1*, 272–298.
11. Morishige, K.; Kacher, D. F.; Libby, P.; Josephson, L.; Ganz, P.; Weissleder, R.; Aikawa, M. High-Resolution Magnetic Resonance Imaging Enhanced with Superparamagnetic Nanoparticles Measures Macrophage Burden in Atherosclerosis/Clinical Perspective. *Circulation* **2010**, *122*, 1707–1715.
12. Daldrup-Link, H. E.; Golovko, D.; Ruffell, B.; DeNardo, D. G.; Castaneda, R.; Ansari, C.; Rao, J.; Tikhomirov, G. A.; Wendland, M. F.; Corot, C.; *et al*. MRI of Tumor-Associated Macrophages with Clinically Applicable Iron Oxide Nanoparticles. *Clin. Cancer Res.* **2011**, *17*, 5695–5704.
13. Luciani, A.; Dechoux, S.; Deveaux, V.; Poirier-Quinot, M.; Luciani, N.; Levy, M.; Ballet, S.; Manin, S.; Péchoux, C.; Autret, G., *et al*. Magnetic Resonance Tracking of Adipose Tissue Macrophages for the Monitoring of Obesity-Associated Inflammation. *Radiology*, in press.
14. Corot, C.; Robert, P.; Idee, J. M.; Port, M. Recent Advances in Iron Oxide Nanocrystal Technology for Medical Imaging. *Adv. Drug Delivery Rev.* **2006**, *58*, 1471–1504.
15. Sigovan, M.; Boussel, L.; Sulaiman, A.; Sappey-Marinier, D.; Alsaid, H.; Desbleds-Mansard, C.; Ibarrola, D.; Gamondes, D.; Corot, C.; Lancelot, E.; *et al*. Rapid-Clearance Iron Nanoparticles for Inflammation Imaging of Atherosclerotic Plaque: Initial Experience in Animal Model. *Radiology* **2009**, *252*, 401–409.
16. Montet-Abou, K.; Daire, J.-L.; Hyacinthe, J.-N.; Jorge-Costa, M.; Grosdemange, K.; Mach, F.; Petri-Fink, A.; Hofmann, H.; Morel, D. R.; Vallée, J.-P.; *et al*. *In Vivo* Labelling of Resting Monocytes in the Reticulo-endothelial System with Fluorescent Iron Oxide Nanoparticles Prior to Injury Reveals That They Are Mobilized to Infarcted Myocardium. *Eur. Heart J.* **2010**, *31*, 1410–1420.
17. Levy, M.; Luciani, N.; Alloyeau, D.; Elgrabli, D.; Deveaux, V.; Pechoux, C.; Chat, S.; Wang, G.; Vats, N.; Gendron, F.; *et al*. Long Term *In Vivo* Biotransformation of Iron Oxide Nanoparticles. *Biomaterials* **2011**, *32*, 3988–3999.
18. Muthana, M.; Giannoudis, A.; Scott, S. D.; Fang, H.-Y.; Coffelt, S. B.; Morrow, F. J.; Murdoch, C.; Burton, J.; Cross, N.; Burke, B.; *et al*. Use of Macrophages to Target Therapeutic Adenovirus to Human Prostate Tumors. *Cancer Res.* **2011**, *71*, 1805–1815.
19. Leuschner, F.; Dutta, P.; Gorbatov, R.; Novobrantseva, T. I.; Donahoe, J. S.; Courties, G.; Lee, K. M.; Kim, J. I.; Markmann, J. F.; Marinelli, B.; *et al*. Therapeutic SiRNA Silencing in Inflammatory Monocytes in Mice. *Nat. Biotechnol.* **2011**, *29*, 1005–1010.
20. McCarthy, J. R.; Korngold, E.; Weissleder, R.; Jaffer, F. A. A Light-Activated Theranostic Nanoagent for Targeted Macrophage Ablation in Inflammatory Atherosclerosis. *Small* **2010**, *6*, 2041–2049.
21. Levy, M.; Wilhelm, C.; Luciani, N.; Devaux, V.; Gendron, F.; Luciani, A.; Devaud, M.; Gazeau, F. Nanomagnetism Reveals the Intracellular Clustering of Nanoparticles in the Organism. *Nanoscale* **2011**, *3*, 4402–4410.
22. Fortin, J. P.; Gazeau, F.; Wilhelm, C. Intracellular Heating of Living Cells through Neel Relaxation of Magnetic Nanoparticles. *Eur. Biophys. J.* **2008**, *37*, 223–228.
23. Mahmoudi, M.; Laurent, S.; Shokrgozar, M. A.; Hosseinkhani, M. Toxicity Evaluations of Superparamagnetic Iron Oxide Nanoparticles: Cell "Vision" *versus* Physicochemical Properties of Nanoparticles. *ACS Nano* **2011**, *5*, 7263–7276.
24. Mahmoudi, M.; Shokrgozar, M. A.; Sardari, S.; Moghadam, M. K.; Vali, H.; Laurent, S.; Stroeve, P. Irreversible Changes in Protein Conformation due to Interaction with Superparamagnetic Iron Oxide Nanoparticles. *Nanoscale* **2011**, *3*, 1127–1138.
25. Rocker, C.; Potzl, M.; Zhang, F.; Parak, W. J.; Nienhaus, G. U. A Quantitative Fluorescence Study of Protein Monolayer Formation on Colloidal Nanoparticles. *Nat. Nanotechnol.* **2009**, *4*, 577–580.
26. Jiang, X.; Weise, S.; Hafner, M.; Rocker, C.; Zhang, F.; Parak, W. J.; Nienhaus, G. U. Quantitative Analysis of the Protein Corona on FePt Nanoparticles Formed by Transferrin Binding. *J. R. Soc., Interface* **2010**, *7*, S5–S13.
27. Petri-Fink, A.; Steitz, B.; Finka, A.; Salaklang, J.; Hofmann, H. Effect of Cell Media on Polymer Coated Superparamagnetic Iron Oxide Nanoparticles (SPIONs): Colloidal Stability, Cytotoxicity, and Cellular Uptake Studies. *Eur. J. Pharm. Biopharm.* **2008**, *68*, 129–137.
28. Wilhelm, C.; Billotey, C.; Roger, J.; Pons, J. N.; Bacri, J. C.; Gazeau, F. Intracellular Uptake of Anionic Superparamagnetic Nanoparticles as a Function of their Surface Coating. *Biomaterials* **2003**, *24*, 1001–1011.
29. Massart, R. Preparation of Aqueous Magnetic Liquids in Alkaline and Acidic Media. *IEEE Trans. Magn.* **1981**, *17*, 1247–1248.
30. Levy, M.; Lagarde, F.; Maraloiu, V. A.; Blanchin, M. G.; Gendron, F.; Wilhelm, C.; Gazeau, F. Degradability of Superparamagnetic Nanoparticles in a Model of Intracellular Environment: Follow-Up of Magnetic, Structural, and Chemical Properties. *Nanotechnology* **2010**, *21*, 395103.
31. Sigovan, M.; Bessaad, A.; Alsaid, H.; Lancelot, E.; Corot, C.; Neyran, B.; Provost, N.; Majd, Z.; Breisse, M.; Canet-Soulas, E. Assessment of Age Modulated Vascular Inflammation in ApoE−/− Mice by USPIO-Enhanced Magnetic Resonance Imaging. *Invest. Radiol.* **2010**, *45*, 702–707.
32. Hasmonay, E.; Dubois, E.; Bacri, J.-C.; Perzynski, R.; Raikher, Y. L.; Stepanov, V. I. Static Magneto-optical Birefringence of Size-Sorted γ-Fe_2O_3 Nanoparticles. *Eur. Phys. J. B* **1998**, *5*, 859–867.
33. Wilhelm, C.; Gazeau, F.; Roger, J.; Pons, J. N.; Salis, M. F.; Perzynski, R.; Bacri, J. C. Binding of Biological Effectors on Magnetic Nanoparticles Measured by a Magnetically Induced Transient Birefringence Experiment. *Phys. Rev. E: Stat., Nonlinear, Soft Matter Phys.* **2002**, *65*, 031404.
34. He, X. M.; Carter, D. C. Atomic Structure and Chemistry of Human Serum Albumin. *Nature* **1992**, *358*, 209–215.
35. Monopoli, M. P.; Walczyk, D.; Campbell, A.; Elia, G.; Lynch, I.; Bombelli, F. B.; Dawson, K. A. Physical-Chemical Aspects of Protein Corona: Relevance to *in Vitro* and *in Vivo* Biological Impacts of Nanoparticles. *J. Am. Chem. Soc.* **2011**, *133*, 2525–2534.
36. Vroman, L.; Adams, A.; Fischer, G.; Munoz, P. Interaction of High Molecular Weight Kininogen, Factor XII, and Fibrinogen in Plasma at Interfaces. *Blood* **1980**, *55*, 156–159.
37. Tenzer, S.; Docter, D.; Rosfa, S.; Wlodarski, A.; Kuharev, J.; Rekik, A.; Knauer, S. K.; Bantz, C.; Nawroth, T.; Bier, C.; *et al*. Nanoparticle Size is a Critical Physicochemical Determinant

of the Human Blood Plasma Corona: a Comprehensive Quantitative Proteomic Analysis. *ACS Nano* **2011**, *5*, 7155–7167.
38. Mahmoudi, M.; Serpooshan, V. Large Protein Absorptions from Small Changes on the Surface of Nanoparticles. *J Phys Chem C* **2011**, *115*, 18275–18283.
39. Jung, S. Y.; Lim, S. M.; Albertorio, F.; Kim, G.; Gurau, M. C.; Yang, R. D.; Holden, M. A.; Cremer, P. S. The Vroman Effect: A Molecular Level Description of Fibrinogen Displacement. *J. Am. Chem. Soc.* **2003**, *125*, 12782–12786.
40. Cedervall, T.; Lynch, I.; Foy, M.; Berggard, T.; Donnelly, S. C.; Cagney, G.; Linse, S.; Dawson, K. A. Detailed Identification of Plasma Proteins Adsorbed on Copolymer Nanoparticles. *Angew. Chem., Int. Ed.* **2007**, *46*, 5754–5756.
41. Lück, M.; Paulke, B. R.; Schröder, W.; Blunk, T.; Müller, R. H. Analysis of Plasma Protein Adsorption on Polymeric Nanoparticles with Different Surface Characteristics. *J Biomed Mater Res* **1998**, *39*, 478–485.
42. Lesniak, A.; Campbell, A.; Monopoli, M. P.; Lynch, I.; Salvati, A.; Dawson, K. A. Serum Heat Inactivation Affects Protein Corona Composition and Nanoparticle Uptake. *Biomaterials* **2010**, *31*, 9511–9518.
43. Ehrenberg, M. S.; Friedman, A. E.; Finkelstein, J. N.; Oberdorster, G.; McGrath, J. L. The Influence of Protein Adsorption on Nanoparticle Association with Cultured Endothelial Cells. *Biomaterials* **2009**, *30*, 603–610.
44. Maiorano, G.; Sabella, S.; Sorce, B.; Brunetti, V.; Malvindi, M. A.; Cingolani, R.; Pompa, P. P. Effects of Cell Culture Media on the Dynamic Formation of Protein-Nanoparticle Complexes and Influence on the Cellular Response. *ACS Nano* **2010**, *4*, 7481–7491.
45. Wilhelm, C.; Gazeau, F.; Bacri, J. C. Magnetophoresis and Ferromagnetic Resonance of Magnetically Labeled Cells. *Eur. Biophys. J.* **2002**, *31*, 118–125.
46. Luciani, N.; Gazeau, F.; Wilhelm, C. Reactivity of the Monocyte/Macrophage System to Superparamagnetic Anionic Nanoparticles. *J. Mater. Chem.* **2009**, *19*, 6373–6380.
47. Zensi, A.; Begley, D.; Pontikis, C.; Legros, C.; Mihoreanu, L.; Büchel, C.; Kreuter, J. Human Serum Albumin Nanoparticles Modified with Apolipoprotein A-I Cross the Blood-Brain Barrier and Enter the Rodent Brain. *J Drug Targeting* **2010**, *18*, 842–848.
48. Walczyk, D.; Bombelli, F. B.; Monopoli, M. P.; Lynch, I.; Dawson, K. A. What the Cell ″Sees″ in Bionanoscience. *J. Am. Chem. Soc.* **2010**, *132*, 5761–5768.
49. Wilhelm, C.; Gazeau, F. Universal Cell Labelling with Anionic Magnetic Nanoparticles. *Biomaterials* **2008**, *29*, 3161–3174.